An Adaptive Threshold Tracking Area Update and Selective Probabilistic Paging Scheme for Signaling Cost Reduction in 5G NR Networks

Kalpesh Popat[1], Divyakant Meva[1], and Hardik K. Molia[2]

[1]*Marwadi University, Rajkot, India,*
[2]*Government Engineering College, Bhavnagar, India*

https://doi.org/10.26636/jtit.2026.3.2701

Submitted: 3 Jul. 2026, Accepted: 26 Aug. 2026

Abstract — Tracking area update (TAU) and paging are two competing signaling-cost characteristics of 5G NR networks: a smaller registration area reduces paging cost but increases TAU signaling and vice versa. The majority of existing schemes optimize one parameter while fixing the other and apply a single network-wide parameterization to all users regardless of their heterogeneous call and mobility patterns. This paper proposes ATAU-SP, a scheme that manages both operations jointly, on a per user equipment (UE) basis: each UE maintains an online estimate of its call-to-mobility ratio (CMR) and triggers a TAU only after an adaptive movement threshold derived by minimizing a per UE cost function, with a dwell-time guard that suppresses boundary ping-pong updates. The network builds a residence-probability distribution from a learned Markov mobility model and pages cells in descending probability rounds up to a delay bound. We derive a closed-form analytical cost model and validate it as a provable upper bound against a custom discrete-event simulator. The results show that a well-tuned TAL scheme is the lowest-cost baseline over most of the moderate CMRs, ATAU-SP-ML attains the lowest cost at high CMR, and plain ATAU-SP is best only at very low CMR. Nonetheless, ATAU-SP variants dominate the classical static, distance-, movement-, and time-based schemes throughout, and both ATAU-SP and TAL require materially less machinery per UE state and network side than a full TAL list distribution subsystem.

Keywords — 5G NR, mobility management, paging, signaling cost, tracking area update

1. Introduction

In an idle or inactive radio state, the user equipment (UE) is not in direct communication with the network, so the network maintains only an approximate, area-level record of the UE's location. Two control plane procedures keep this record usable: the first, tracking area update (TAU), is initiated by the UE when it moves into a tracking area that is not included in its list of currently registered tracking area identifiers (TAI). The other, i.e., paging, is initiated by the network when downlink traffic arrives for an idle UE, as the access and mobility management function (AMF) broadcasts a paging message across the cells of the UE's registration area until the UE responds. Together, these procedures constitute location management.

If a UE registers its location frequently, the network knows its position precisely, and paging is cheap, but TAU signaling is high. If registration is infrequent, TAU signaling falls, but the network must page a larger area to locate the UE. Because both procedures consume scarce control plane and radio resources and, on the UE side, battery energy, minimizing their combined cost is a long-standing objective that has only gained in importance as network density increases and massive numbers of low-power devices join the network [1]–[3].

Despite previous work, three limitations still exist. First, most schemes treat the two operations separately: they fix the registration rule and then optimize paging, or vice versa. Second, schemes typically apply a single network-wide parameterization to all UEs, even though real populations are highly heterogeneous: a stationary metering device, a pedestrian, and a vehicle differ by orders of magnitude in both mobility rate and call frequency, so a parameter that is optimal on average is suboptimal for most individual UEs. Surveys of 5G mobility management identify adaptive, per-UE, prediction-assisted location management as an open direction [1].

A third limitation is that per-UE adaptive schemes have rarely been benchmarked against per-UE tracking area list (TAL) schemes or against learning-based next-cell predictors under a common cost model. Both are per UE, so the comparison is not obvious.

This paper addresses these limitations with ATAU-SP – a joint, adaptive, per-UE location management scheme, and provides an empirical comparison against the two baseline families identified above.

The scientific contribution is as follows:

- Jointly adaptive scheme. ATAU-SP couples an adaptive registration with a probability-ordered paging rule, so that the registration threshold and the paging search are optimized together against a single signaling cost objective.

This work is licensed under a Creative Commons Attribution 4.0 International (CC BY 4.0) License.
For more information, see https://creativecommons.org/licenses/by/4.0/

- Per-UE adaptive movement threshold with a formally characterized estimator. Each UE estimates its own call-to-mobility ratio (CMR) using an exponentially weighted moving average (EWMA) and sets its TAU threshold by minimizing a closed-form per-UE cost function. This paper adds a convergence analysis of the EWMA estimator – a bias half-life and a steady-state noise floor, both in closed form – and quantifies how estimation error propagates to the threshold through the cube-root relationship.
- Selective probabilistic paging under a delay bound, with an explicit grouping rule and an entropy-based benchmark. Upon the arrival of a call, AMF builds a residence probability distribution over candidate cells and pages them in descending probability rounds, subject to a hard limit D_{max} on the number of rounds. This article explicitly states the probability-balanced grouping rule and compares the realized mean delay against an information-theoretic lower bound.
- Two additional baselines and comparison. We implement and simulate a dynamic, frequency-based TAL scheme and a lightweight second-order Markov predictor ATAU-SP-ML, alongside the original four baselines, and report where each of them wins, rather than only where ATAU-SP wins.
- Analytical model, simulation validation, and new sensitivity analysis. We develop a closed-form per-UE cost expression, validate it as a provable upper bound against a custom discrete event simulator (DES), and add a cost-ratio sensitivity sweep, a dwell-time-guard ablation, a Markov matrix learning convergence study, and a UE-energy proxy grounded in a published TAU power measurement.

The remainder of this paper is organized as follows. Section 2 reviews related work. Section 3 presents a model of the system and the formulation of the problem. Section 4 describes the ATAU-SP algorithm, including TAL and ATAU-SP-ML. Section 5 derives the analytical cost model. Section 6 describes the simulation setup. Section 7 reports and discusses the results. Section 8 concludes the article.

2. Related Works

2.1. Registration Strategies (Location Update)

Registration strategies fall into those of the static and dynamic category. Static strategies group cells into fixed location or tracking areas. A UE registers only when it crosses an area boundary, and the network pages the entire area. The area size is a network-wide design parameter, which makes static schemes simple but not capable of adapting to the behavior of individual UEs. Dynamic strategies make the registration decision specific to the UE. The three canonical dynamic rules are distance-based, movement-based, and time-based.

Research shows that each rule has an optimal threshold that depends on the ratio between call arrival rate and mobility rate, and that the distance-based rule is generally the most efficient of the three but the hardest to implement, as it requires the UE to compute distance in cells [1], [4], [5].

More recent work targets the 5G tracking-area structure directly. Dynamic TAL schemes assign each UE a personalized list of tracking areas to balance TAU and paging overhead, and clustering-based methods group cells into tracking areas according to observed intercell mobility, so that frequently traversed boundaries fall inside a tracking area rather than across one [6], [7].

2.2. Paging Strategies

Paging strategies range from blanket parallel paging, which pages all cells of the registration area simultaneously to minimize delay at maximum signaling cost, to sequential paging, which pages cells one group at a time to minimize signaling cost at the expense of delay. Selective and probabilistic paging methods order the search by the estimated probability that the UE resides in each cell.

Searching in descending order of probability minimizes the expected number of cells paged. Delay-bounded variants partition the area into a fixed number of paging rounds, so that the worst-case delay is controlled while still exploiting the probability ordering [5], [8], [9].

2.3. Mobility Prediction for Location Management

Mobility prediction is the foundation of the residence probabilities that selective paging and adaptive registration require. Markov models are widely used because they rely only on information already available to the network, such as handover and cell-residence history. Their low complexity is a contributing factor as well.

Weighted and user-classified Markov models improve precision by accounting for the heterogeneity of individual movement patterns rather than relying on a single aggregate model [10]. Classical movement-based location-update and selective-paging schemes have also been studied as joint location-management mechanisms [11].

Machine learning approaches, including hidden Markov models and neural sequence models, can capture a longer-range structure at a higher computational cost [5], [12], [13]. Recent work adopted a first-order Markov model as a lightweight predictor and was cited, but did not implement a learning-based alternative.

2.4. Optimization-based and Learning-based Mobility Management

A parallel line of research formulates cell tracking area or reporting planning as an NP-hard combinatorial optimization problem and solves it with metaheuristics such as genetic algorithms, particle swarm optimization, and related methods [14], [15], or with learning-based controllers that adapt the configuration to traffic [16], [17].

Comprehensive surveys of 5G and beyond mobility management catalog these directions and highlight adaptive, prediction-assisted, and energy-aware location management as priorities, particularly for ultra-dense deployments and large device populations [1], [3], [19], [20].

Machine learning for handover and mobility optimization reaches similar conclusions about the value of adaptation [12], [13]. Independently of location management specifically, large-scale studies of real human mobility using call-detail record (CDR) and GPS data report that individuals repeatedly return to a small number of frequently visited locations and that a large share of individual trajectories is theoretically predictable [21], [22].

3. System Model and Problem Formulation

ATAU-SP differs from the above in that it adapts both the registration decision and the paging search jointly and per-UE, against a single cost objective, while remaining lightweight enough for network-side implementation.

The classical static, distance-based, movement-based, and time-based schemes, as well as blanket paging, all arise as special cases of ATAU-SP, which lets us argue dominance rather than incomparable difference for that family of baselines.

Against the two per-UE baselines – a dynamic personalized TAL and a higher-order Markov predictor – ATAU-SP does not dominate uniformly; their relative performance depends on the operating regime.

3.1. Network and Mobility Model

Service area is modeled as a set of N hexagonal cells $C = \{c_1, \ldots, c_N\}$, each served by one gNB, with a fixed inter-site distance (Fig. 1). Cells are grouped into tracking areas (Fig. 2).

The number of cells per tracking area s is a configurable parameter. We focus on idle mode UEs, whose location is known to the network at tracking area granularity. The UE population is U.

For a UE u, cell residence times are independent and identically distributed with a mean $1/\lambda_m(u)$, so that the cell crossing (mobility) rate is $\lambda_m(u)$. The next sessions (calls) arrive as a Poisson process with a rate of $\lambda_c(u)$ [18]. The per-UE call-to-mobility ratio is defined as:

$$CMR(u) = \frac{\lambda_c(u)}{\lambda_m(u)} \,. \tag{1}$$

A low CMR denotes a highly mobile UE that is rarely called (favoring infrequent registration), and a high CMR denotes a frequently called, slowly moving UE (favoring frequent registration).

The movement of UE at the cell level is described by a first-order Markov chain with a transition matrix

$$P = [p_{ij}] \,,$$

where P_{ij} is the probability that an UE in cell c_i next enters cell c_j. The matrix is estimated from observed intercell transitions, optionally weighted by UE class to reflect heterogeneous movement patterns [10].

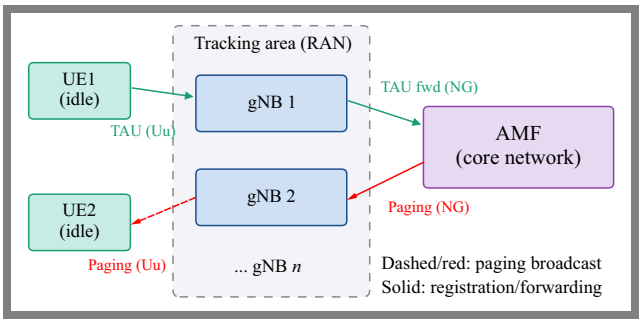


Fig. 1. 5G NR location management model. An idle UE registers via TAU over the Uu and NG interfaces. On a call, the AMF triggers paging across the registration area.

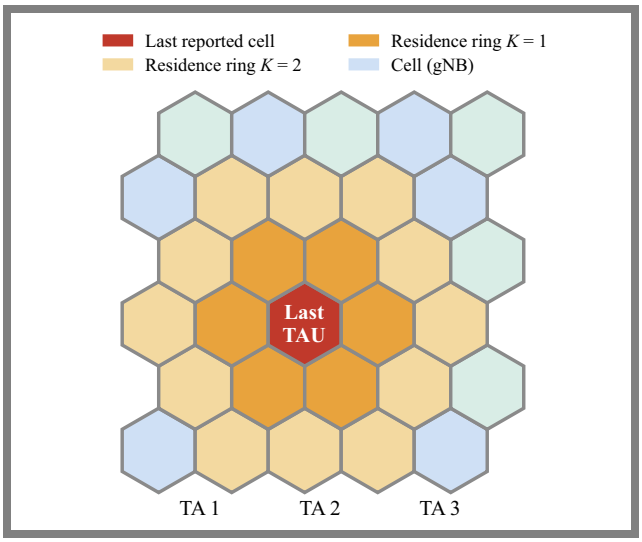


Fig. 2. Hexagonal cells grouped into tracking areas. After up to K crossings since the last TAU, the UE lies within a residence neighborhood of K rings around the last reported cell.

3.2. Cost Model

Let C_u be the signaling cost of one TAU and C_p the signaling cost of paging one cell. Over a long observation window, the per-UE signaling cost rate is the sum of a registration term and a paging term:

$$\Phi(u) = C_u \cdot R(u) + C_p \cdot \lambda_c(u) \cdot M(u) \,, \tag{2}$$

where $R(u)$ is the UE's TAU rate (updates per unit time), and $M(u)$ is the expected number of cells paged per incoming call. The first term is the registration cost, and the second is the paging cost, since each call triggers a search over $M(u)$ cells on average. Both $R(u)$ and $M(u)$ depend on the registration and paging rules.

The network-wide objective is to minimize total cost subject to a paging delay constraint:

$$\begin{gathered} \text{minimize} \sum_{u \in U} \Phi(u) \text{ subject to} \\ D(u) \leqslant D_{max} \text{ and } P_{succ}(u) \geqslant \rho \end{gathered} \,, \tag{3}$$

where $D(u)$ is the delay in paging in rounds, D_{max} is the maximum allowed number of paging rounds, $P_{succ}(u)$ is the probability that the UE is found within the delay bound, and ρ is target success probability.

Because UEs are independent in this model, the network objective decomposes into independent per-UE problems, which is what makes per-UE adaptation both tractable and beneficial – a property shared by the TAL and ATAU-SP-ML baselines introduced below, both of which are also per-UE schemes.

4. Proposed ATAU-SP Algorithm and Baseline Extensions

ATAU-SP consists of two coupled mechanisms: an adaptive-threshold registration rule executed at the UE, and a selective probabilistic paging rule executed at the network. Both are driven by quantities that are already observable in a 5G NR system, namely cell-crossing events, call arrivals, and inter-cell transition statistics.

This section also specifies the dwell-time-guard hysteresis rule, the probability-balanced grouping procedure and introduces the two new baselines: a dynamic TAL scheme and a second-order Markov predictor ATAU-SP-ML.

4.1. Adaptive-threshold Tracking-area Update

Each UE maintains an estimate of its CMR using an EWMA of its observed cell-crossing and call-arrival intervals:

$$\dot{m}(u) = \alpha \cdot \tau_m + (1-\alpha) \cdot \dot{m}(u) \,,$$

$$\dot{c}(u) = \alpha \cdot \tau_c + (1-\alpha) \cdot \dot{c}(u) \,,$$

where τ_m and τ_c are the most recently observed intercrossing and inter-call intervals, giving the following:

$$\hat{C}MR(u) = \frac{\dot{m}(u)}{\dot{c}(u)} \,.$$

The UE counts cell crossings since its last TAU. When the count reaches an adaptive threshold $K(u)$, it issues a TAU and resets the count. A dwell-time guard suppresses a TAU if the crossing is an immediate return to the previously visited cell within one crossing interval. If the newly entered cell is equal to the cell the UE occupied two crossings ago, the crossing is not counted toward k and no TAU is triggered.

The threshold $K(u)$ is set by minimizing the per-UE cost and is recomputed whenever $\hat{C}MR(u)$ changes by more than a fixed tolerance 15%. Setting $K(u)$ to a fixed constant recovers the classical movement-based scheme, and keying the count to the hop distance from the last registered cell recovers the distance-based scheme. ATAU-SP makes the threshold state-dependent and per-UE instead.

4.2. Selective Probabilistic Paging

When a call arrives for an idle UE, the AMF computes a residence probability vector over the candidate cells in the UE registration area (Fig. 3). Starting from the last reported cell and the crossings elapsed since the last TAU, the network propagates the learned Markov chain to obtain, for each candidate cell c_j, a residence probability π_j. Candidate cells are sorted in descending order π_j and partitioned into D_{max} paging rounds at most.

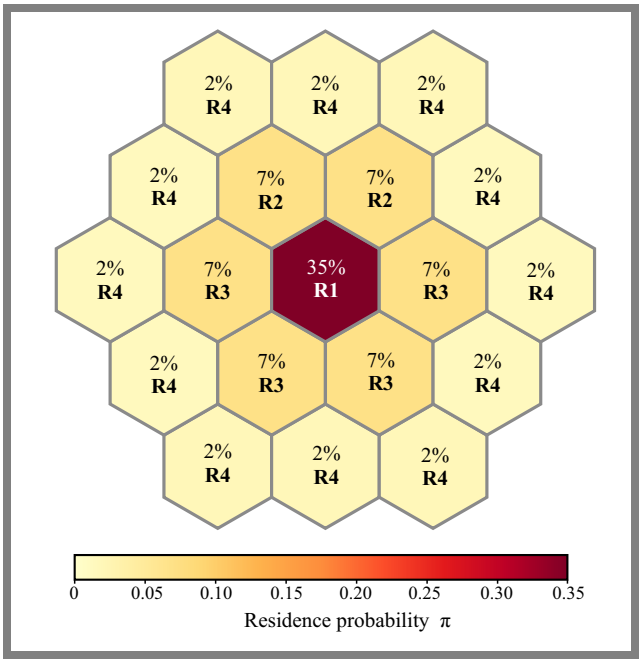


Fig. 3. Selective probabilistic paging. Candidate cells are shaded by residence probability and paged in descending probability rounds $(\mathrm{R1}, \mathrm{R2}, \ldots)$ up to the delay bound D_{max}, reducing the expected number of cells paged relative to blanket paging.

The AMF pages the first round. If the UE does not respond, it pages the second round and so on, stopping as soon as the UE responds or the bound D_{max} is reached. Setting $D_{max} = 1$ with all cells in a single round recovers blanket parallel paging, allowing one cell per round recovers maximum likelihood sequential paging.

The structure of the algorithm is as follows (Fig. 4).

Procedure 1 – Adaptive registration (runs on each UE).

1) Initialize crossing counter $k \leftarrow 0$ and CMR estimate from a warm-up window.
2) In each cell crossing, update the mobility rate EWMA. For setting the dwell-time guard, if the newly entered cell equals the cell occupied two crossings ago, i.e., the UE has bounced back to where it just came from, do not increment k and return without further action.
3) Otherwise increment k. If $k \geqslant K(u)$, issue a TAU carrying the current cell, then reset $k \leftarrow 0$.
4) On each incoming call, update the call rate EWMA, recompute $\hat{C}MR(u)$ and, if it has changed by more than 15% since the last recomputation, recompute $K(u)$.

Procedure 2 – Network-side selective paging (runs at the AMF).

5) On a call for idle UE u, retrieve the last reported cell and the crossing count since the last TAU, propagate the Markov chain that many steps to obtain residence probabilities π over the candidate cell set $A = ring_K$(last reported cell). The set of cells that can be reached in most K hops

$$|A| = f(K).$$

6) Probability-balanced grouping. Sort candidate cells by descending π. Partition the sorted list into D_{max} consec-

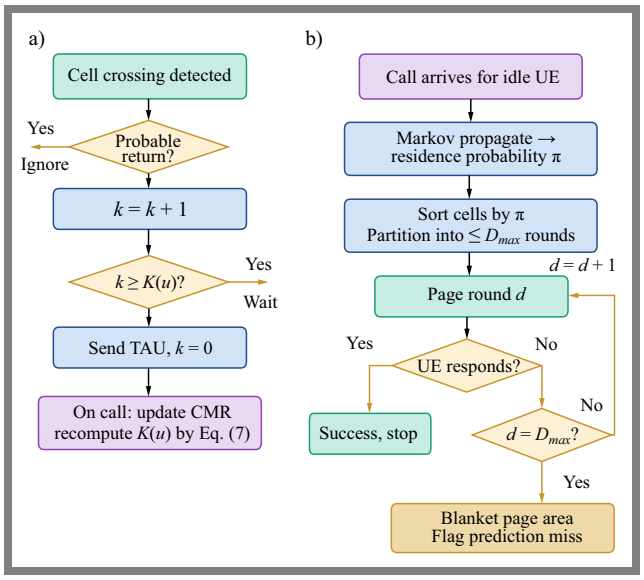


Fig. 4. ATAU-SP control flow scheme: a) adaptive registration procedure with dwell-time guarding and online threshold recomputation, and b) selective probabilistic paging procedure on the network side with descending probability rounds and a blanket paging fallback.

utive groups $g_1, \ldots, g_{D_{max}}$ of as equal a size as possible, i.e.

$$|g_j| = \lceil |A|/D_{max} \rceil$$

for the first $|A|$ mod D_{max} groups and $\lfloor |A|/D_{max} \rfloor$ thereafter, so that

$$\sum_j |g_j| = |A|.$$

This is the instantiation of the "probability-balanced grouping" by Eq. (5), where g_j denotes the number of cells assigned to paging round j according to this rule.

7) For round $d = 1$ to D_{max}, page the cells of round d, i.e.,

$$\sum_{j \leqslant d} g_j$$

reduces to exactly g_d being paged at step d, having not paged earlier rounds cells again. If the UE responds, record success and stop. The cumulative number of cells grouped by round d is

$$\sum_{j \leqslant d} |g_j|,$$

which is the $M(K)$ term in Eq. (5).

8) If there is no response after D_{max} rounds, fall back to blanket paging of the full registration area and flag a prediction miss for model update.

Procedure 1 costs $O(1)$ per event, apart from threshold recomputation, which is a one-dimensional minimization with a closed-form solution. Procedure 2 costs $O(|A| \log |A|)$ per call for sorting $|A|$ candidate cells of the registration area, plus the Markov propagation, which is sparse because the transition matrix has non-zero entries only between adjacent cells. Both are lightweight enough for online use.

4.3. TAL Scheme

We implement a dynamic TAL scheme in the style of [7]. Each UE is assigned a personalized list of cells (its TAL) rather than a network-fixed tracking area. The network maintains an online, per-UE visit frequency table over the cells. Whenever the UE crosses into a cell outside its current TAL, it issues a TAU. In this scheme, the TAU also implicitly requests a list refresh, so TAU and list update signaling are counted together at the same C_u cost, giving TAL no advantage over ATAU-SP's registration cost accounting.

Once the visit frequency table for the local neighborhood has accumulated enough observations, the network rebuilds the TAL as the UE's most frequently visited cells within an expanded radius of the new anchor cell, up to a size budget matched to $f(K_{radius})$ for a radius parameter tuned relative to the same movement-threshold scale. Before the table has warmed up, the list returns to a simple geometric neighborhood. Paging, when a call arrives, pages the UE's entire current TAL at once.

Note that our synthetic mobility models are memoryless or weakly correlated random walks without repeated visitation structure, for example, with no modeled "home" and "work" anchor cells, so a frequency-based list under these traces converges to a geometric neighborhood of the recently visited cells.

4.4. ATAU-SP-ML, a Second-order Markov Predictor

We implement a second-order (bigram) Markov model that conditions the next predicted cell based on the current cell and the cell visited immediately before it, learned online from the same crossing events already available to the first-order model, with a one-cell-of-history requirement that can be piggybacked on existing TAU signaling.

ATAU-SP equipped with this predictor is referred to as ATAU-SP-ML. It uses the same adaptive threshold registration and round-based paging as ATAU-SP, differing only in how the residence-probability vector π is computed.

5. Analytical Cost Model

We derive the per-UE cost as a function of the registration threshold K and then obtain the optimal threshold. Between two successive calls, the expected number of cell crossings is equal to the ratio of the mobility rate to the call rate

$$\frac{\lambda_m}{\lambda_c} = \frac{1}{CMR}.$$

With a movement threshold K, the UE issues one TAU every K crossings, so the expected number of TAUs per call cycle is

$$\frac{1}{CMR \cdot K},$$

and the registration cost per call cycle is (Fig. 5):

$$\Phi_{reg}(K) = C_u \cdot \frac{1}{CMR \cdot K}. \quad (4)$$

On the paging side, after up to K crossings since the last TAU, the UE lies within a neighborhood of the last reported

cell whose size grows with K. For a hexagonal layout, the number of cells within K rings is

$$f(K) = 3K(K+1) + 1 \, .$$

Under blanket paging, the paging cost per call is $C_p \cdot f(K)$. Under ATAU-SP selective paging, ordering cells by residence probability and applying the probability-balanced grouping of Sec. 4.2 reduces the expected number of cells paged to:

$$M(K) = \sum_{d=1}^{D_{max}} \left(\sum_{j \leqslant D} |g_j| \right) \cdot q_d \, , \tag{5}$$

where $|g_j|$ is the number of cells assigned to paging round j by the equal-count partition of procedure 2, step 6, and q_d is the probability that the UE is first located in round d.

The cells are searched in descending probability order, $M(K) \leqslant f(K)$, with equality only when the residence distribution is uniform. By the rearrangement inequality, no other ordering of the candidate cells yields a smaller expected search, so descending probability paging is optimal for a given partition into rounds.

Combining the cost two terms, the per call cycle is:

$$\Phi(K) = \frac{C_u}{CMR \cdot K} + C_p \cdot M(K) \, . \tag{6}$$

The first term decreases in K, while the second increases in K, so a unique minimizer exists. $M(K)$ is approximated by a quadratic in K, since $f(K)$ is quadratic, and selective paging scales it by a near-constant factor over the operating range. Setting the derivative to zero gives an optimal threshold of the form:

$$K^* = \kappa \cdot \left(\frac{C_u}{C_p \cdot CMR} \right)^{\frac{1}{3}} . \tag{7}$$

Equation (7) is the analytical basis for the adaptive rule: K^* increases as CMR decreases, so highly mobile, rarely called UEs register less often, while frequently called UEs register more often (Fig. 6). ATAU-SP substitutes the online estimate $CMR(u)$ in Eq. (7), clip K^* to the integer range admissible for the size of the registration area and applies it on the per-UE basis. The constant κ is set by a numerical sweep of the fixed K cost simulated at the $CMR = 1$, $C_u : C_p = 10 : 1$, which locates the true empirical minimum at $K = 2$ and gives $\kappa = 0.93$.

5.1. Convergence of the CMR Estimator

Both $\dot{m}(u)$ and $\dot{c}(u)$ are EWMA estimates of the mean of an exponentially distributed inter-event time. Two standard properties of the exponential smoothing estimator characterize its behavior.

The first is bias decay from a cold start. If the estimator is initialized at a value that differs from the true rate by a factor of β, the relative bias after n observed events decays as $(1-\alpha)^n$. Therefore, the bias half-life is:

$$t_{1/2} = \frac{\ln 2}{-\ln(1-\alpha)} \, ,$$

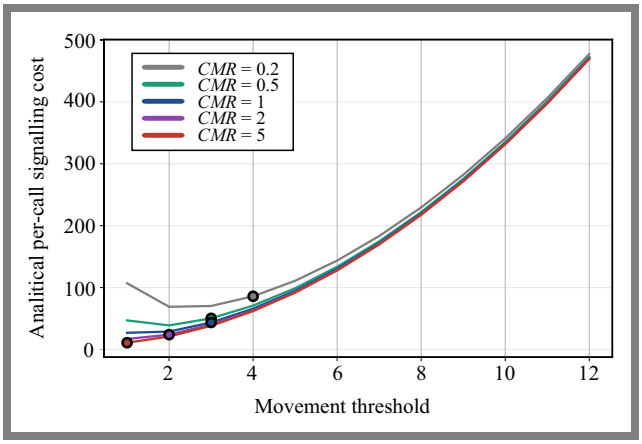


Fig. 5. Analytical cost per call of signaling cost $\Phi(K)$ vs. movement threshold K for several CMRs, evaluated from Eq. (6) with $f(K) = 3K(K+1)+1$ and $C_u : C_p = 20$. The cost is convex in K; circles mark the optimal threshold K^*, using $\kappa = 0.93$.

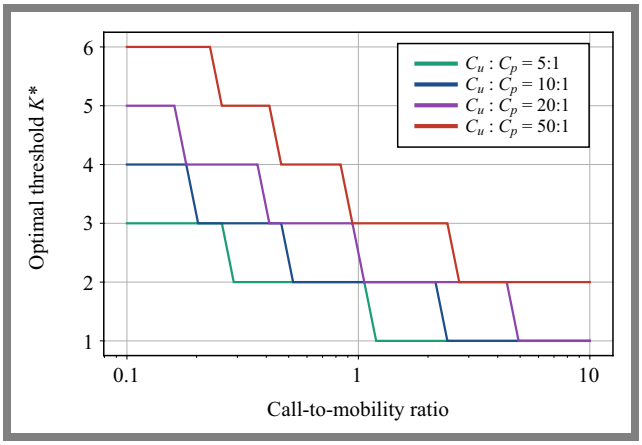


Fig. 6. Analytical optimal threshold K^* vs. call-to-mobility ratio for several cost ratios, from Eqs. (6)–(7).

events and the number of events needed to shed 90% of the initial bias is:

$$n_{90\%} = \frac{\ln 0.1}{\ln(1-\alpha)} \, .$$

For $\alpha = 0.1$, these give $t_{1/2} \approx 6.6$ events and $n_{90\%} \approx 21.9$ events – i.e., a warm-up window of roughly 20 crossing/call events per UE is sufficient for the cold start bias to become negligible.

The second is steady-state noise floor. Because the smoothed quantity is itself a noisy per-event sample rather than a converging average, EWMA retains an irreducible steady-state variance even after the bias has decayed. For an exponential inter-event time $CV = 1$, the steady state relative error of the EWMA estimate is approximately:

$$\sqrt{\frac{\alpha}{2-\alpha}} \, ,$$

combining the mobility- and call-rate estimates via the ratio $\hat{C}MR = \dot{m}/\dot{c}$ roughly doubles this value in the worst case. We verified both properties with a synthetic Monte Carlo test (300 trials, 5× mismatched cold start): the measured steady-state error was 18%, 26–30%, and 37–42% for α = 0.05,

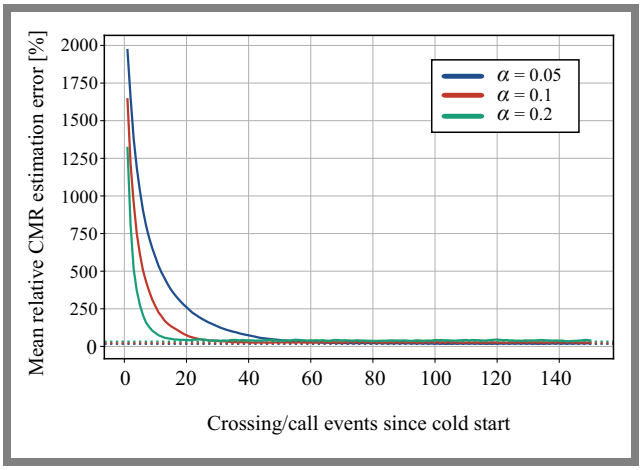


Fig. 7. EWMA-CMR convergence: mean relative estimation error vs. number of observed events, for three decay rates α, starting from a 5× mismatched cold start. The dotted lines mark the closed-form steady-state noise floor.

0.1, and 0.2 respectively, consistent with the closed-form floor.

Figure 7 plots the measured convergence curves. This smaller α gives a lower noise floor (more precise threshold selection) but is slower to track a genuinely time-varying CMR, e.g., a UE that changes its mobility pattern, while larger α tracks changes faster at the cost of noisier, more frequent threshold recomputation. We use α = 0.1 throughout, balancing a sub-30-event warm-up against a moderate 26 – 30% steady-state floor.

Consider the error propagation to the threshold from Eq. (7), a first-order propagation gives relative error in $K^* \approx 1/3\times$ relative error in $\hat{C}MR$. Therefore, the cube root relationship is self-damping: even a 26 – 30% steady-state CMR estimation error at α = 0.1 propagates to an error of approximately 9 – 10% only in K^*, and because K^* is subsequently clipped to a small integer range, the realized threshold values are often completely unaffected by estimation noise.

5.2. Paging Delay Bound and Theoretic Comparison

For a residence distribution π over $|A| = f(K)$ candidate cells with Shannon entropy $H(\pi)$, a standard argument for grouped sequential search states that no grouping into D_{max} rounds can achieve the expected number of rounds below:

$$\frac{H(\pi)}{\log_2(|A|/D_{max})},$$

where $|A|/D_{max}$ is the average branching factor of a round. This is an approximate bound in our setting, but it gives a basic floor to compare against. Using the simulator, the mean entropy of the residence distribution at the moment of call $CMR = 1, \sim 18$ cells/TA is $H(\pi) \approx 3.45$ bits on a mean candidate-set size of 14.2 cells. With $D_{max} = 3$, this gives a lower bound of approximately 1.54 rounds. The simulated mean delay at $D_{max} = 3$ is 1.76 rounds, about 14% above this bound, indicating that the simple equal-count grouping used by ATAU-SP operates reasonably close to, but measurably short of, the entropy-optimal grouping, which would require unequal-size rounds rather than the equal-count rule currently used.

5.3. Quadratic Approximation Error and Its Propagation

Fixing K and running the simulator gives the true simulated $M(K)$ at each integer K. Fitting the least squares-optimal scalar γ in the surrogate

$$M_{quad}(K) = \gamma \times f(K)$$

against these measured points shows that the point-wise fit is loose. At $CMR = 1$ the relative error is

$$\frac{|M(K) - M - quad(K)|}{M(K)}$$

and ranges from 3.5% near $K = 5$ to 76.6% at $K = 1$, averaging 39.8% across $K = 1 - 6$. This is consistent with, and helps explain, the 46.5% average envelope gap reported in Sec. 7.9. The quadratic surrogate is a genuinely loose local approximation to the true selective-paging cost, not merely a small correction.

Whether this loose pointwise fit changes the resulting threshold choice is a separate question, and the answer is operating-point dependent. Comparison of the argmin of Eq. (6) against the argmin of the quadratic surrogate at $CMR = 1$ and $CMR = 5$, the two curves select the same integer $K^* = 2$ and $K^* = 1$ respectively. Despite the large pointwise $M(K)$ error, the resulting threshold and cost are unaffected – the registration term's $1/K$ divergence at small K dominates the argmin decision at these points, and the fit error is not large enough to shift it.

At $CMR = 0.5$, however, the quadratic surrogate does select a different threshold from the true optimum ($K^*_{quad} = 3$ vs. $K^*_{exact} = 2$), and using the surrogate threshold in practice would incur a measurable, if modest, cost penalty of 2.3% relative to the true optimum. Therefore, the quadratic approximation's threshold selection error is real but small where it occurs. We observed a value of 2.3% at most across the three CMR values tested. It does not occur at every operating point and the closed form remains useful for the qualitative CMR dependence of Eq. (7).

6. Simulation Setup

ATAU-SP and six baselines were implemented in a custom discrete-event simulator written in Python (vectorized with NumPy). The simulator models location management at the signaling level: cells are nodes of a hexagonal adjacency graph, the UE's serving cell is updated by a direction-persistent random walk on that graph calibrated per mobility model, while cell crossings and call arrivals are generated as independent Poisson processes with per-UE rates $\lambda_m(u), \lambda_c(u)$ [23].

The logic runs the registration procedure of Sec. 4.2; a central function plays the role of the AMF, holding each UE's last reported cell, learning the Markov transition matrix (or matrices, for ATAU-SP-ML) from observed crossings, exe-

Tab. 1. Simulation parameters.

Parameter	Value
Simulator	Custom Python (NumPy) discrete-event, signaling-level
Topology	37 hexagonal cells, one gNB per cell
Inter-site distance	500 m
Cells per tracking area	5, 7, 12, 18, 37 (operating point ≈ 18)
Number of UEs	100 (idle mode), heterogeneous CMR (log-normal, $\sigma = 0.6$)
Mobility models	Random waypoint; Gauss-Markov (heading persistence $\kappa = 0.75$); RPGM (5 groups of 20)
UE speed	1 – 30 m/s (default 10)
Call arrivals	Poisson, per-UE rate set to the UE's target CMR × mobility rate
CMR	0.1 – 10 (nominal, population mean)
Cost ratio $C_u : C_p$	10:1 nominal; swept 5:1, 10:1, 20:1, 50:1
Paging delay bound D_{max}	1 – 5 (default 3)
Markov model order	ATAU-SP and bigram ATAU-SP-ML
TAL list size budget	$f(radius)$, $radius = \max(1, \lfloor K/2 \rfloor)$, frequency-ranked
K^* calibration constant κ	0.93
Simulation time / step	1200 s / event-driven (Poisson inter-event sampling), 200 s warm-up
Replications	15 (main sweeps), 8 – 12 (secondary sweeps), 95% CIs reported

cuting the paging procedure, and tallying signaling statistics. TAU and paging are modeled as counted control events.

Correlated mobility is generated at the cell-graph level rather than by simulating continuous positions. At each mobility event, the UE's heading persists with probability $\kappa = 0$ for random waypoint, $\kappa = 0.75$ for Gauss-Markov, and a two-level group/member persistence model for RPGM (group-anchor heading persistence 0.85, member-to-anchor attraction 0.55), so that the sequences of visited cells among group members exhibit correlation.

This is a coarser abstraction than simulating continuous UE positions and is explicitly stated as a modeling simplification. Such an approach preserves the qualitative ordering of the prediction difficulty across the three models (RWP is the hardest to predict, RPGM the easiest).

All schemes are implemented in the same module and evaluated under identical topologies, mobility traces, and call traces, so that differences are attributable to the schemes alone:

- Static registration area + blanket paging – the 3GPP-style reference: register at the boundary crossing, page the whole area at once.

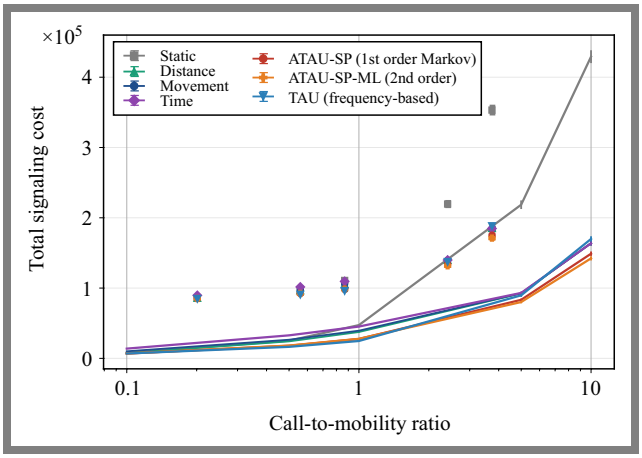


Fig. 8. Total signaling cost vs. CMR for all seven schemes (random waypoint, ≈ 18 cells/TA), including the TAL and ATAU-SP-ML baselines.

- Distance-based + blanket paging – register after a threshold hop distance from the last registered cell.
- Movement-based + blanket paging – register after a fixed number of cell crossings.
- Time-based + blanket paging – register after a fixed time interval.
- ATAU-SP (proposed) – adaptive per-UE threshold with first-order Markov selective probabilistic paging.
- ATAU-SP-ML – identical registration and round-based paging as ATAU-SP, using the second-order (bigram) Markov predictor.
- TAL – dynamic, frequency-based personalized tracking area list with blanket paging over the current list.

The performance metrics are as follows:

- TAU rate (updates per UE per unit time) and total registration signaling.
- Mean cells paged per call (paging signaling).
- Total signaling cost under a sweep of the cost ratio $C_u : C_p$.
- Paging success probability within the delay bound and mean paging delay (rounds), compared against an entropy-based lower bound.
- Convergence of the CMR estimator.
- Dwell-time-guard contribution, isolated by ablation.
- UE energy proxy (idle-mode monitoring plus TAU transmissions), grounded in a published per-TAU power measurement.

7. Results and Discussion

All results below are produced using parameters listed in Tab. 1.

7.1. Total Signaling Cost versus CMR

Comparison against the four classical baselines (static, distance, movement, and time) shows that ATAU-SP outperforms all four at every CMR tested. At $CMR = 1$, ATAU-SP

Tab. 2. Total signaling cost (normalized units) vs CMR, random waypoint, ≈ 18 cells/TA (mean over 15 seeds). The lowest values per row are shown in bold.

CMR	Static	Distance	Movement	Time	ATAU-SP	ATAU-SP-ML	TAL
0.1	7812	7492	10 034	13 865	**6808**	6947	6909
0.5	25 137	24 181	26 492	32 739	17 930	18 222	**16 382**
1.0	47 329	37 503	39 361	45 252	27 578	27 815	**24 708**
5.0	218 594	92 313	92 669	93 105	83 298	**80 128**	89 683
10.0	429 221	163 830	163 904	163 746	148 915	**142 275**	169 898

Tab. 3. TAU rate and mean cells paged per call at $CMR = 1$ (random waypoint, ≈ 18 cells/TA). The lowest total cost is shown in bold.

Scheme	TAU rate [UE/s]	Cells paged / call	Total cost
Static	0.00378	17.58	44 608
Distance	0.00572	13.11	36 181
Movement	0.00786	12.98	38 009
Time	0.01391	13.03	44 174
ATAU-SP	0.00786	8.07	26 608
ATAU-SP-ML	0.00786	8.19	26 875
TAL	0.00849	6.68	**24 016**

reduces signalling cost by 26.5% compared with the best classical dynamic baseline (distance-based) and by 41.8% compared with static registration, corresponding to an average reduction of approximately 34.1% across these two reference schemes (Fig. 8)..

TAL is the lowest cost scheme from $CMR = 0.5$ through $CMR = 1$ (8.6 – 10.4% below plain ATAU-SP), plain ATAU-SP is the cheapest only at the lowest CMR tested (0.1), where paging is rarely invoked and TAL's list refresh overhead is not yet amortized, and ATAU-SP-ML becomes the cheapest at high CMR (5 and 10), by 3.8% and 4.5% over plain ATAU-SP and by 10.7% and 16.3% over TAL, respectively.

7.2. Registration and Paging Overhead Decomposition

The decomposition shows that the per-UE schemes outperform the classical baselines and why TAL edges out ATAU-SP at this operating point (Tab. 3). Static registers rarely (once per 264 UE-seconds) the largest area (17.6 cells/call).

The classical dynamic schemes cut paging to roughly 13 cells/call at the cost of more frequent registration. ATAU-SP and ATAU-SP-ML have the same TAU rate as movement-based approaches, since both use the same adaptive-threshold registration rule, while cutting paging even further, to 8.1 to 8.2 cells/call, via probability-ordered rounds.

TAL achieves the lowest paging cost of all: 6.68 cells/call, since it bounds the search to a small personalized list rather than a K-ring neighborhood at a marginally higher TAU rate (0.00849 vs. 0.00786/UE/s) than the movement threshold schemes, and the net effect is the lowest total cost specified in this table.

This demonstrates that a well-tuned personalized list can outperform threshold-based adaptive registration under conditions where paging cost dominates.

7.3. Effect of the Registration-area Size

The crossover between static and the per-UE schemes now falls between 7 and 12 cells/TA, below which static is cheaper and above which every per-UE scheme (ATAU-SP, ATAU-SP-ML, and TAL alike) is cheaper (Fig. 9).

At the dense deployment operating point of 18 cells/TA, TAL is 46.8% below static and ATAU-SP is 40.9% below static. At 37 cells/TA, the gaps widen to 72.7% and 69.4% respectively.

Since 5G deployments trend toward larger tracking-area configurations to limit TAU signaling from massive device populations, the large-area regime where per-UE schemes win is the operationally relevant one, and this conclusion is robust to the choice of per-UE scheme.

7.4. Effect of Mobility Model

Qualitative ranking is consistent across random waypoint, Gauss-Markov, and RPGM approaches: TAL is the lowest in all three, closely followed by ATAU-SP and ATAU-SP-ML, with classical dynamic baselines being 30 – 34% higher and static being 42 – 46% higher (Fig. 10).

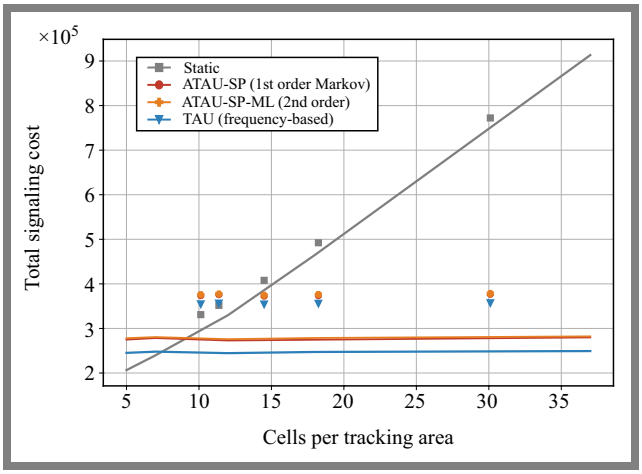


Fig. 9. Total cost vs. size of the tracking area for static, ATAU-SP, ATAU-SP-ML, and TAL (random waypoint, $CMR = 1$).

Tab. 4. Total signaling cost versus cost ratio for $CMR = 1$, random waypoint, ≈ 18 cells/TA. The lowest values per row are shown in bold.

$C_u : C_p$	Static	Distance	Movement	Time	ATAU-SP	ATAU-SP-ML	TAL
5:1	44 488	26 791	27 438	28 983	21 546	21 286	**20 383**
10:1	46 456	37 516	39 520	45 599	27 409	27 697	**24 575**
20:1	50 488	47 612	52 526	68 312	35 789	36 344	**32 760**
50:1	59 324	63 129	76 479	123 718	51 171	**51 963**	51 279

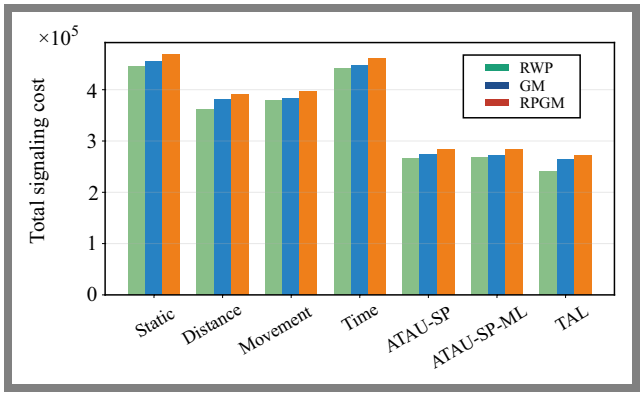


Fig. 10. Total cost under the three mobility models for all seven schemes ($CMR = 1, \approx 18$ cells/TA).

The second-order predictor's advantage is primarily a high-CMR effect in this simulator, not primarily a mobility-correlation effect.

7.5. Effect of UE Speed

As UE speed increases from 1 to 30 m/s, cell-crossing frequency and, hence, signaling cost increase for every scheme, but the relative ranking is stable throughout the swept range (Fig. 11). TAL is the lowest at every speed (by 19.4% over plain ATAU-SP at 1 m/s, narrowing to 2.5% at 30 m/s as list-refresh overhead grows with crossing frequency), with ATAU-SP and ATAU-SP-ML following close behind and remaining consistently 26 to 33% below the best classical dynamic baseline.

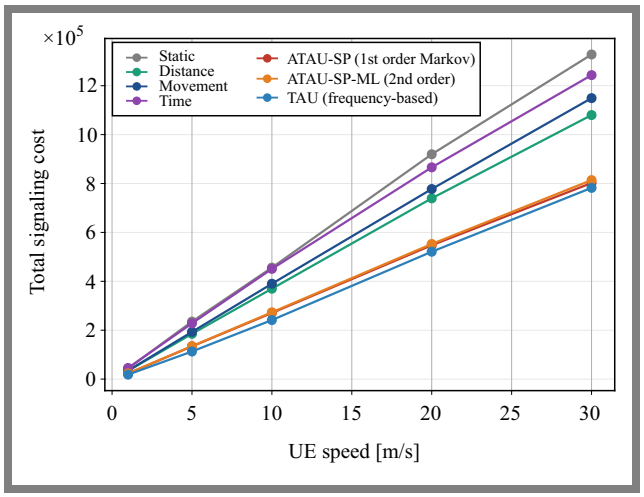


Fig. 11. Total signaling cost vs. UE speed for all seven schemes (random waypoint, $CMR = 1$).

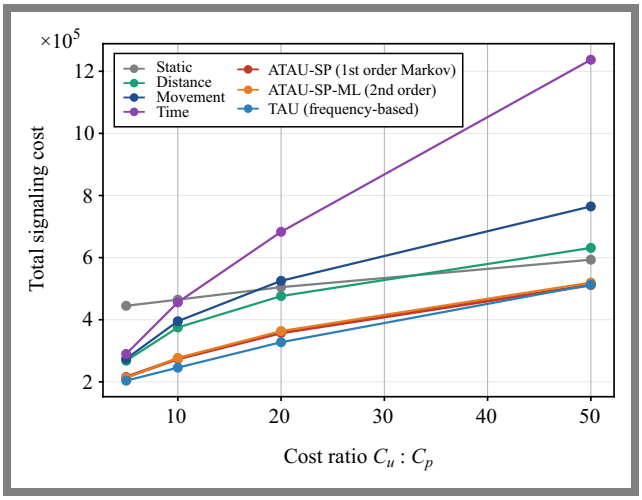


Fig. 12. Total cost vs. cost ratio.

All per-UE schemes remain far below their static and time-based counterparts across the full pedestrian-to-vehicular range. TAL remains the lowest-cost per-UE scheme throughout the swept speed range, while ATAU-SP and ATAU-SP-ML follow closely behind and remain consistently 26–33% below the best classical dynamic baseline.

7.6. Sensitivity to the Registration/Paging Cost Ratio

Table 4 and Fig. 12 show that TAL is the lowest-cost scheme at 5:1, 10:1, and 20:1, but its margin over ATAU-SP narrows sharply as the ratio grows: from 5.4% at 5:1 to essentially a statistical tie at 50:1, where registration cost dominates so heavily that all per-UE schemes with similar TAU rates converge. At 50:1, plain ATAU-SP is in fact marginally the lowest (51 171 vs. TAL's 51 279, a 0.2% difference well within simulation noise).

Classical dynamic baselines (distance, movement, time) degrade badly at high-cost ratios. the time-based approach, is 2.4× more expensive than ATAU-SP at 50:1, since its fixed time interval does not adapt to the increased penalty for registering.

7.7. Paging Delay Bound and an Entropy-based Comparison

Figure 13 illustrates that sweeping D_{max} from 1 to 5 traces the delay-cost trade-off, with the mean delay rises from 1.00 round (blanket paging) to 2.65 rounds, while total cost falls from 39 153 at $D_{max} = 1$ to 26 984 at $D_{max} = 3$, with a further small reduction to 26 038 at $D_{max} = 4$, before

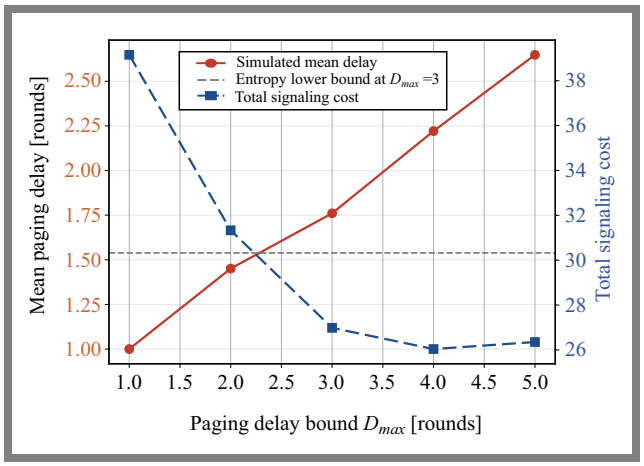


Fig. 13. ATAU-SP total cost and mean paging delay vs. D_{max} delay bound.

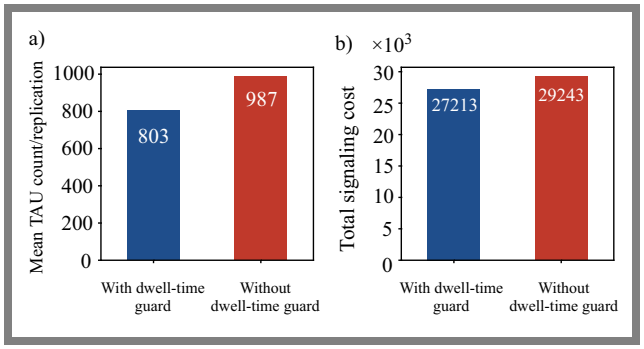


Fig. 14. Dwell-time-guard ablation: TAU count a) and total cost with and without the guard b).

a marginal increase to 26 352 at $D_{max} = 5$. This confirms the choice of $D_{max} = 3$ as a reasonable default on empirical grounds.

The lower bound for $D_{max} = 3$ is approximately 1.54 rounds versus a simulated value of 1.76 rounds – the simple equal-count probability-balanced grouping used by ATAU-SP is within about 14% of the theoretical floor.

7.8. Algorithm Parameter Analysis

The dwell-time guard and the online learning of the Markov transition matrix were previously described only qualitatively. Now, we isolate each by ablation/instrumentation.

At $CMR = 1$, random waypoint, 18 cells/TA, running ATAU-SP with the guard disabled increases the mean TAU count per replication from 803.3 to 987.5 (+22.9%) and increases the total cost from 27 213 to 29 243 (+7.5%). The guard suppresses a mean of 407.8 immediate boundary return crossings per replication that would otherwise each have counted toward the movement threshold and, over a sufficient number of them, triggered spurious TAUs (Fig. 14).

7.9. Model Validation

The simulator's selective, probability-ordered paging achieves $M(K) \leqslant f(K)$ by design, so the analytical curve is expected to sit above the simulated curve at every point (Fig. 15). It does so at the five CMR values tested, with an average gap

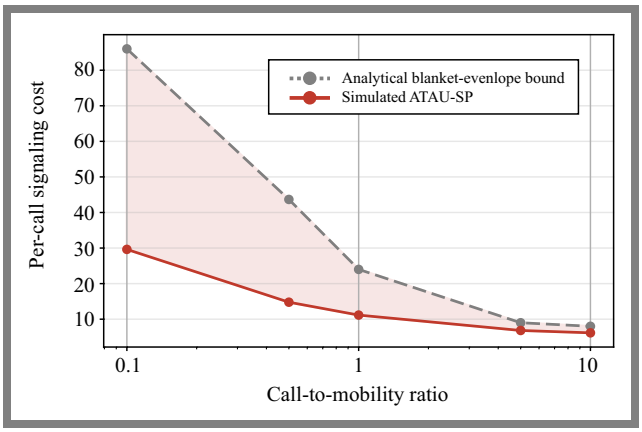


Fig. 15. Analytical blanket envelope bound.

Tab. 5. Total signaling cost: static partitions ($CMR = 1$, RWP). The lowest value per row is shown in bold.

Cells/TA	Static (geometric)	Static (clustered)	ATAU-SP	TAL
5	**20 494**	20 544	27 126	24 470
12	32 587	33 239	27 126	**24 470**
18	45 762	37 377	27 126	**24 470**
37	88 262	88 262	27 126	**24 470**

of 46.5% (ranging from 23.0% in $CMR = 10$ to 66.2% at $CMR = 0.5$). We report this as an envelope gap, not a prediction error.

Equation (6) is validated as a correct, non-trivial upper bound and the gap size quantifies how much selective, learned-probability paging saves over the blanket bound. Because the underlying UE-side and AMF-side operations are $O(1)$ and $O(|A| \log |A|)$, total signaling still scales nearly linearly with the number of UEs, independently of this correction.

To assess whether ATAU-SP is lightweight enough for online use in energy terms, we built a simple, transparently assumption-laden proxy rather than a full energy simulator.

According to [21], a single TAU procedure drains approximately 10 mW of UE battery power, assuming a NAS+RRC exchange duration of approximately 0.5 s. This gives an energy cost of approximately 5 mJ per TAU.

Under this proxy, the relative consumption of UE energy across the schemes tracks their TAU rate and is marginally higher (0.00849/UE/s, ≈ 4.2 µJ/UE/s), while that of the time-based approach is markedly worse (0.01391/UE/s, ≈ 7.0 µJ/UE/s, roughly 77% more TAU energy than ATAU-SP). Note, this is a coarse, explicitly caveated proxy, not a validated power model.

At a dense deployment operating point (18 cells/TA), flow-aware clustering reduces the static approach's cost by 18.3% relative to the geometric partition (37 377 vs. 45 762), confirming that clustering does capture a real, exploitable structure (Tab. 5).

It does not, however, close the gap to the per-UE schemes: clustered static remains 34.5% above TAL and 27.4% above ATAU-SP at this operating point. At 12 cells/TA, the clustered

Tab. 6. Energy-aware threshold selection vs. the network-cost-optimal threshold ($CMR = 1$, RWP, ≈ 18 cells/TA).

Scheme	ATAU-SP (network cost optimal K)	ATAU-SP, energy-aware K
TAU rate [UE/s]	0.00781	0.00438
Network cost	26 659	33 716
UE energy proxy [mJ/UE]	39.07	21.91

partition is marginally worse than the geometric one (33 239 vs. 32 587, a 2.0% increase) – at small tracking-area sizes, the greedy flow-based merge does not reliably outperform simple geometric contiguity, and we report this small negative result rather than only the favorable ones.

At 5 and 37 cells/TA, the two partitions are effectively identical. Overall, clustering offers a genuine improvement over the static baseline, but does not change this paper's central finding that per-UE adaptive schemes (ATAU-SP, ATAU-SP-ML, TAL) dominate any single network-wide partition.

The energy-aware variant cuts the UE energy proxy by 43.9% (39.07 to 21.91 mJ/UE) at the expense of a 26.5% increase in network signaling cost (26 659 to 33 716 – Tab. 6). This is a quantified trade-off rather than a free win, and it is the trade-off that an energy-aware scheme is supposed to make.

8. Conclusions

This paper presented ATAU-SP – a joint, adaptive, per-UE location management scheme for 5G NR that couples an adaptive-threshold registration rule with selective probabilistic paging under a delay bound and with two baselines: a dynamic, frequency-based tracking-area-list (TAL) scheme and a lightweight second-order Markov predictor (ATAU-SP-ML), together with a cost-ratio sensitivity sweep, a formal CMR-estimator convergence analysis, a dwell-time-guard ablation, an entropy-based comparison for the paging delay bound, and a UE energy proxy.

ATAU-SP and ATAU-SP-ML outperform the four classical baselines (static, distance, movement, and time) at every operating point tested. At the nominal operating point, ATAU-SP reduces total signalling cost by approximately 26.5% compared with the best classical dynamic baseline (distance-based) and by 40.4% compared with static registration, while ATAU-SP-ML achieves reductions of approximately 25.7% and 39.8%, respectively. These improvements remain consistent across the mobility-model, speed, area-size, and cost-ratio sweeps. Against the newly implemented TAL baseline, however, ATAU-SP is not uniformly the best: a well-tuned dynamic TAL scheme is the lowest-cost option across the majority of the moderate-to-high call-to-mobility range and across the full swept cost-ratio range. ATAU-SP-ML overtakes it at high CMR (5 – 10), while plain ATAU-SP is the cheapest at very low CMR only.

Future work will focus on improving paging-round grouping and making K^*calibration operating-point-specific or fully data-driven, eliminating the need for a fixed constant κ. We will validate the model using real cell-level carrier mobility traces, including behavioral revisitation patterns, and reassess TAL under such realistic mobility. We will also develop a validated UE energy model that accounts for the state-maintenance costs of ATAU-SP-ML bigram counts and the TAL frequency table, and replace the assumed 0.1 mJ paging-response energy with a measured value. Further work will examine self-similar and Markov-modulated call arrivals, broader CMR-heterogeneity distributions, and beam-level paging in directional NR.

Acknowledgments

The full discrete-event simulator, all driver scripts, result files, and figures are publicly available at https://github.com/kapopat1980/atau.

References

[1] S.M.A. Zaidi, M. Manalastas, H. Farooq, and A. Imran, "Mobility Management in Emerging Ultra-dense Cellular Networks: A Survey, Outlook, and Future Research Directions", *IEEE Access*, vol. 8, pp. 183505–183533, 2020 (https://doi.org/10.1109/ACCESS.2020.3027258).

[2] A. Sufyan *et al.*, "From 5G to Beyond 5G: A Comprehensive Survey of Wireless Network Evolution, Challenges, and Promising Technologies", *Electronics*, vol. 12, art. no. 2200, 2023 (https://doi.org/10.3390/electronics12102200).

[3] Y. Ullah *et al.*, "A Survey on Handover and Mobility Management in 5G HetNets: Current State, Challenges, and Future Directions", *Sensors*, vol. 23, art. no. 5081, 2023 (https://doi.org/10.3390/s23115081).

[4] A. Bar-Noy, I. Kessler, and M. Sidi, "Mobile Users: To Update or Not to Update?", *Wireless Networks*, vol. 1, pp. 175–185, 1995 (https://doi.org/10.1007/BF01202540).

[5] A.G. Chekol and M.S. Fufa, "A Survey on Next Location Prediction Techniques, Applications, and Challenges", *EURASIP Journal on Wireless Communications and Networking*, vol. 2022, art. no. 29, 2022 (https://doi.org/10.1186/s13638-022-02114-6).

[6] H. Jang and J. Baek, "Optimal TAL-based Registration with Cell-based Central Policy in Mobile Cellular Networks: A Semi-Markov Process Approach", *The Journal of Supercomputing*, vol. 77, pp. 9172–9189, 2021 (https://doi.org/10.1007/s11227-021-03624-8).

[7] M. Bagaa, T. Taleb, and A. Ksentini, "Efficient Tracking Area Management Framework for 5G Networks", *IEEE Transactions on Wireless Communications*, vol. 15, pp. 4117–4131, 2016 (https://doi.org/10.1109/TWC.2016.2535217).

[8] W.-K. Choi and J.-Y. Pyun, "Machine Learning-based Paging Enhancement in 5G Network", *Applied Sciences*, vol. 12, art. no. 9555, 2022 (https://doi.org/10.3390/app12199555).

[9] C. Rose and R. Yates, "Minimizing the Average Cost of Paging Under Delay Constraints", *Wireless Networks*, vol. 1, pp. 211–219, 1995 (https://doi.org/10.1007/BF01202543).

[10] M. Yan *et al.*, "Mobility Prediction Using a Weighted Markov Model Based on Mobile User Classification", *Sensors*, vol. 21, art. no. 1740, 2021 (https://doi.org/10.3390/s21051740).

[11] I.F. Akyildiz, J.S.M. Ho, and Y.-B. Lin, "Movement-based Location Update and Selective Paging for PCS Networks", *IEEE/ACM Transactions on Networking*, vol. 4, pp. 629–638, 1996 (https://doi.org/10.1109/90.532871).

[12] S.K. Thillaigovindhan *et al.*, "A Comprehensive Survey on Machine Learning Methods for Handover Optimization in 5G Networks", *Electronics*, vol. 13, art. no. 3223, 2024 (https://doi.org/10.3390/electronics13163223).

[13] M. S. Mollel *et al.*, "A Survey of Machine Learning Applications to Handover Management in 5G and Beyond", *IEEE Access*, vol. 9, pp. 45770–45802, 2021 (https://doi.org/10.1109/ACCESS.2021.3067503).

[14] B. Sapkota *et al.*, "5G Network Deployment Planning Using Meta-heuristic Approaches", *Telecom*, vol. 5, pp. 588–608, 2024 (https://doi.org/10.3390/telecom5030030).

[15] B.B. Haile, E. Mutafungwa, and J. Hämäläinen, "A Data-driven Multiobjective Optimization Framework for Hyperdense 5G Network Planning", *IEEE Access*, vol. 8, pp. 169423–169443, 2020 (https://doi.org/10.1109/ACCESS.2020.3023452).

[16] M. Al-Khalidi, R. Al-Zaidi, and M. Hammoudeh, "Network Mobility Management Challenges, Directions, and Solutions: An Architectural Perspective", *Electronics*, vol. 11, art. no. 2696, 2022 (https://doi.org/10.3390/electronics11172696).

[17] H. Riaz, S. Öztürk, and A. Çalhan, "A Robust Handover Optimization Based on Velocity-aware Fuzzy Logic in 5G Ultra-dense Small Cell HetNets", *Electronics*, vol. 13, art. no. 3349, 2024 (https://doi.org/10.3390/electronics13173349).

[18] J. Navarro-Ortiz *et al.*, "A Survey on 5G Usage Scenarios and Traffic Models", *IEEE Communications Surveys & Tutorials*, vol. 22, pp. 905–929, 2020 (https://doi.org/10.1109/COMST.2020.2971781).

[19] A. Haghrah, M.P. Abdollahi, H. Azarhava, and J.M. Niya, "A Survey on the Handover Management in 5G-NR Cellular Networks: Aspects, Approaches and Challenges", *EURASIP Journal on Wireless Communications and Networking*, vol. 2023, art. no. 52, 2023 (https://doi.org/10.1186/s13638-023-02261-4).

[20] I.F. Akyildiz *et al.*, "Mobility Management in Next-generation Wireless Systems", *Proceedings of the IEEE*, vol. 87, pp. 1347–1384, 1999 (https://doi.org/10.1109/5.775420).

[21] A.A.R. Alsaeedy and E.K.P. Chong, "Tracking Area Update and Paging in 5G Networks: A Survey of Problems and Solutions", *Mobile Networks and Applications*, vol. 24, pp. 578–595, 2019 (https://doi.org/10.1007/s11036-018-1160-6).

[22] M.C. González, C.A. Hidalgo, and A.-L. Barabási, "Understanding Individual Human Mobility Patterns", *Nature*, vol. 453, pp. 779–782, 2008 (https://doi.org/10.1038/nature06958).

[23] T. Camp, J. Boleng, and V. Davies, "A Survey of Mobility Models for Ad Hoc Network Research", *Wireless Communications and Mobile Computing*, vol. 2, pp. 483–502, 2002 (https://doi.org/10.1002/wcm.72).

[24] C. Song, Z. Qu, N. Blumm, and A.-L. Barabási, "Limits of Predictability in Human Mobility", *Science*, vol. 327, pp. 1018–1021, 2010 (https://doi.org/10.1126/science.1177170).

Kalpesh Popat, Ph.D.
Faculty of Computer Applications
https://orcid.org/0000-0002-3818-3717
E-mail: kapopat@gmail.com
Marwadi University, Rajkot, India
https://www.marwadiuniversity.ac.in

Divyakant Meva, Ph.D.
Faculty of Computer Applications
https://orcid.org/0000-0001-8804-7337
E-mail: divyakant.meva@marwadieducation.edu.in
Marwadi University, Rajkot, India
https://www.marwadiuniversity.ac.in

Hardik K. Molia, Ph.D.
Computer Engineering Department
https://orcid.org/0000-0002-1962-7255
E-mail: hardik.molia@gmail.com
Government Engineering College, Bhavnagar, India
https://gecbhavnagar.ac.in